Proton and neutron knockout from ^{36}Ca

R. Shane,* R. J. Charity, and L. G. Sobotka
Departments of Physics and Chemistry, Washington University, St. Louis, Missouri 63130, USA

D. Bazin, B. A. Brown, A. Gade, G. F. Grinyer,† S. McDaniel, A. Ratkiewicz, and D. Weisshaar
National Superconducting Cyclotron Laboratory, Michigan State University, East Lansing, Michigan 48824, USA

A. Bonaccorso
Istituto Nazionale di Fisica Nucleare, Sezione di Pisa, I-56127 Pisa, Italy

J. A. Tostevin
Department of Physics, Faculty of Engineering and Physical Sciences, University of Surrey, Guildford, Surrey GU2 7XH, United Kingdom
(Received 29 March 2012; published 15 June 2012)

The cross sections for single-nucleon knockout from ^{36}Ca on a ^{9}Be target at 70 MeV/nucleon were measured to be $\sigma_{\rm exp}(-p) = 51.1 \pm 2.6$ mb for proton knockout and $\sigma_{\rm exp}(-n) = 5.03 \pm 0.46$ mb for neutron knockout. The spectroscopic factors and orbital angular momenta of the neutrons and protons removed from ^{36}Ca, leading to bound $A = 35$ residues, were deduced by comparison of the experimental cross sections and longitudinal-momentum distributions to those calculated in an eikonal reaction theory, and found to be $S(p, 1d_{3/2}) = 0.79 \pm 0.04$ and $S(n, 2s_{1/2}) = 0.23 \pm 0.02$ (relative to independent-particle-model values and only including experimental contributions to the uncertainties). As found in previous knockout studies, the spectroscopic factor deduced for the deeply bound neutron was significantly reduced relative to shell-model calculations, a result at variance with dispersive optical model (DOM) extrapolations, which suggest a spectroscopic factor closer to 60% of the independent-particle-model value.

DOI: 10.1103/PhysRevC.85.064612 PACS number(s): 24.50.+g, 21.10.Jx, 25.70.Hi, 27.30.+t

I. INTRODUCTION

While the occupancies of single-particle (sp) orbits or their spectroscopic strength at discrete energies are not direct experimental observables [1,2], they are quantities with a clear, almost model-independent interpretation as long as the strength in question is close to the Fermi surface [3]. Plausible reaction models coupled with structure calculations can provide estimates of nucleon-knockout cross sections. If experimental cross sections were to be reproduced, support would then be found for both models. When experimental cross sections are not reproduced, as is found for knockout from deeply bound valence states [4,5], both the reaction and structure calculations must be questioned.

For example, when considering electron-induced knockout reactions [i.e., $(e,e'p)$, on beta-stable nuclei] one finds that the distorted-wave impulse approximation (DWIA), coupled with a Green's function approach to structure calculations, can accurately reproduce the experimental cross sections, lending credence to both the reaction and structure models [3]. These reactions have shown that for beta-stable nuclei there is roughly a 35% universal reduction in spectroscopic strength relative to independent-particle-model (IPM) values.

Similarly, it is thought that eikonal models of light-nucleus-induced nucleon-knockout reactions at intermediate energy can be used to extract spectroscopic strength. The agreement of the extracted spectroscopic strength from the light-nucleus-induced knockout with the $(e,e'p)$ results for beta-stable nuclei has encouraged an effort in the last decade to extend this type of knockout analysis to radioactive nuclei to understand how spectroscopic strength changes off beta stability [6].

From this effort, deviations have been found between the experimental knockout cross sections ($\sigma_{\rm exp}$) and those predicted ($\sigma_{\rm thy}$) from the combination of reaction theory and the shell model (SM). These deviations are quantified most simply by reduction factors $R_s \equiv \frac{\sigma_{\rm exp}}{\sigma_{\rm thy}}$, where $\sigma_{\rm thy} \sim S_{\rm SM}\sigma_{\rm sp}$ is the product of the SM spectroscopic factor and the single-particle cross section for the orbital. In nuclei near the driplines, these reduction factors are slightly less than 1 for the removal of weakly bound valence nucleons, and far less than 1 for the removal of strongly bound valence nucleons [5]. A reduction factor of less than 1 is indeed expected, as it is well known that SM calculations overestimate the localized spectroscopic strength [3]. However, the latter result (with R_s values as small as 0.24 [4]) does not yet have a quantitative explanation.

If the concept of a spectroscopic factor (SF) is still valid for such strongly bound valence nucleons, and if the reaction model is valid, then the small reduction factors suggest a spectroscopic strength far less than the SM estimate in the truncated model space. If one has confidence in the radial overlap function, then the reduction factor fixes the quantity

*Present address: National Superconducting Cyclotron Laboratory, Michigan State University, East Lansing, Michigan 48824, USA.
†Present address: GANIL, CEA/DSM-CNRS/IN2P3, Bvd Henri Becquerel, 14076 Caen, France.

$\frac{S_{\text{deduced}}}{S_{\text{SM}}}$, the ratio between the spectroscopic factor deduced from the experimental data with input from the reaction model (S_{deduced}), and the SM spectroscopic factor (S_{SM}). One interpretation of the small knockout cross sections is a strong, neutron-proton asymmetry-dependent fragmentation of spectroscopic strength due to enhanced correlations—correlations beyond those of the standard shell-model calculation, truncated to a single major shell and without explicit consideration of correlations between the strongly bound particles and nucleons of the opposite isospin projection near the continuum.

The asymmetry dependence of SFs has also been studied with the dispersive optical model (DOM) [7–9] and transfer reactions [10,11]. In the DOM, the optical potential is constrained by data from elastic scattering at positive energies and from electron-induced proton-removal reactions at negative energies. In such an analysis of Ca isotopes [9], a slight reduction of proton spectroscopic factors with increasing neutron content (^{40}Ca to ^{48}Ca) was observed and essentially no change was observed in the neutron spectroscopic factors over the same isotope range. In extrapolating to the dripline, one must keep in mind that the present DOM analyses are only constrained by scattering and bound-state data for *stable* nuclei.

The third line of investigation, transfer experiments on argon isotopes [11], as well as a global analysis of previous neutron-transfer data [10], has also led to the conclusion that there is little change in the strength of neutron correlations with changing neutron content. However, it must be mentioned that the statistical significance of the difference between the trends inferred from transfer and knockout reactions has been questioned [12]. This recent reanalysis of the transfer data finds larger uncertainties in the extracted spectroscopic factors.

Nevertheless, there remain interesting differences between the conclusions drawn from light-nucleus-induced knockout and those drawn from DOM extrapolations to the driplines. The proton-rich nucleus ^{36}Ca is a good testing ground to study this discrepancy since it has both weakly bound and strongly bound valence nucleons ($S_p = 2.57$ MeV and $S_n = 19.3$ MeV [13]) with only one bound state—the ground state—in each of the knockout residues (which simplifies the analysis considerably) and there exist DOM extrapolations from a robust data set [9]. The latter suggest spectroscopic factors relative to IPM values[1] of $S_{\text{DOM}}(n, 2s_{1/2}) \approx 0.60-0.65$ and $S_{\text{DOM}}\left(p, 1d_{3/2}\right) \approx 0.7-0.8$ (the range accounts for the estimated uncertainty in linear and isospin symmetry conserving extrapolations). In contrast, the published systematic trends from light-target-nucleus-induced knockout reactions (assuming the validity of the reaction model and the removed nucleon's radial wave function) suggest a neutron SF two to three times smaller.

[1]Others have called these renormalization coefficients of spectroscopic strength z factors (see Ref. [18]). This definition of spectroscopic factors is equal to the spectroscopic factors employed in the Macfarlane and French sum rules [19] for nucleon addition, while for nucleon removal (from a full subshell with spin j) they are equal to spectroscopic factors (obeying the Macfarlane and French sum rules) divided by the occupancy $(2j + 1)$. This division removes a largely irrelevant orbital detail and makes the spectroscopic factors always less than 1. This definition of spectroscopic factors is used in, for example, Ref. [20].

II. EXPERIMENT

Nucleon-knockout experiments were performed at the National Superconducting Cyclotron Laboratory (NSCL) on the campus of Michigan State University. The proton-rich nucleus ^{36}Ca ($t_{1/2} = 102$ ms) was produced by fragmenting a 140 MeV/nucleon ^{40}Ca primary beam on a ^{9}Be target and was filtered using the A1900 fragment separator [14]. This yielded a cocktail beam of $N = 16$ isotones with an average midtarget energy of ∼70 MeV/nucleon. The ^{36}Ca purity was 8%, and other beam constituents included ^{35}K, ^{34}Ar, ^{33}Cl, and ^{32}S. This secondary beam was delivered to the knockout target, a 188 mg/cm^2-thick ^{9}Be foil located at the target position of the S800 spectrograph [15].

The CsI(Na) gamma-ray spectrometer CAESAR [16] was placed around the Be target position of the S800 to observe the decay of any excited states formed in the knockout reaction. Knockout residues were identified and tracked through the S800 on an event-by-event basis. Two position-sensitive cathode-readout drift chambers (CRDCs) measured the residue position in the S800 focal plane, and an ionization chamber (IC) measured energy loss [17]. Reaction identification is done in two steps: one must first identify the incoming particle and then identify the residues coming from reactions involving that incoming particle.

The ion time of flight (TOF) between the focal plane (XFP) of the A1900 and the object position (OBJ) of the S800 provides the separation of the incoming isotones. The selected ions have fixed rigidity $\frac{mv}{q}$ (and are fully stripped of electrons so that $q = Z$). Thus the velocity increases with increasing Z and the TOF decreases. Outgoing reaction residues are identified in a two-dimensional (2-D) plot of the TOF through the S800 versus the energy loss (dE) in the S800 IC detector. One only needs to identify a single residue in this plot and then follow lines of isotopes or isotones to identify the remaining residues.

The complete reaction identification consists of a software gate on the incoming particle and a gate on the reaction residue in the TOF-dE map. The residue identification was confirmed using CAESAR data for those nuclides with known gamma rays.

III. RESULTS

A. Gamma-ray spectra

The CAESAR array is used to identify gamma rays from knockout to bound excited states of the residues and to correct for any excited-state feeding of the ground state, if present. Since the proton separation energy of ^{35}K is only 84 keV [13], it is likely that there are no bound excited states and thus no gamma rays from excited-state decay were expected nor were any observed.

For ^{35}Ca, the proton separation energy has the much larger value of 1.28 MeV [13]. This allowed window for excited states

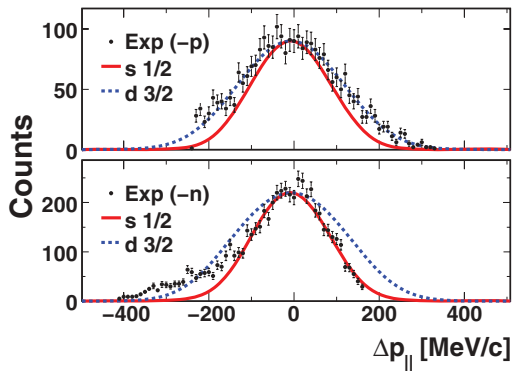

FIG. 1. (Color online) Longitudinal-momentum distributions (in the rest frame of the projectile) for the residues of the following reactions on ^{36}Ca: (top) proton knockout to ^{35}K and (bottom) neutron knockout to ^{35}Ca. Experimental data are given by the points. Also shown are eikonal/HF calculations for $l = 0$ (solid curve) and $l = 2$ (dashed curve), normalized to the experimental peak height.

is substantially less than the excitation of the 2.39 MeV first excited state in its analog ^{35}P [13]. Thus it was again expected that no particle-stable excited states would be observed and this was confirmed by the CAESAR data.

B. Longitudinal-momentum distributions

The shape of the longitudinal-momentum distribution of the residues is characteristic of the angular momentum of the knocked-out nucleon—the larger the orbital angular momentum of the sp state, the larger the momentum dispersion of the residue after a nucleon is removed from this orbit. The IPM leads one to expect that the valence neutrons in ^{36}Ca occupy an $s_{1/2}$ orbital, and the protons occupy a $d_{3/2}$ orbital, so that knocked-out neutrons will have $l = 0$ and protons will have $l = 2$.

The experimentally observed distributions are displayed in Fig. 1 for both the proton- and neutron-knockout reactions from ^{36}Ca, along with eikonal/Hartree-Fock (HF) calculations (described in Sec. IV) for the removal of nucleons with $l = 0$ (solid curve) and $l = 2$ (dashed curve), normalized to the experimental peak height. A comparison between the experimental and calculated distributions (folded with the experimental resolution, determined from the momentum width of the unreacted beam) confirms the IPM expectations. As has been seen in other data sets, the longitudinal momentum distribution from the removal of the deeply bound neutrons has a low-momentum tail that is not reproduced by eikonal models, which do not include explicit energy conservation and the dynamical effects of transfer of energy to the target.

C. Knockout cross sections

Cross sections were determined on a run-by-run basis initially to check for inconsistencies. Results from the individual runs agreed fairly well [e.g., for the neutron knockout the rms deviation from the average cross section was 0.7 mb (14%) and is comparable to the statistical uncertainty of each run, which was around 0.6 mb (11%)]. The data were then aggregated to improve the statistics. The resulting cross sections (shown in Table I) were $\sigma_{\rm exp}(-p) = 51.1 \pm 2.6$ mb for proton knockout and $\sigma_{\rm exp}(-n) = 5.03 \pm 0.46$ mb for neutron knockout.

For the proton knockout, an extrapolation was used to account for the cutoff of the low-momentum tail (left side in Fig. 1). The quoted uncertainties include a contribution from the target thickness uncertainty (2%). For the neutron knockout, there is also included a systematic uncertainty of 4% due to a small discrepancy between unreacted-beam reference runs taken before and after the reaction runs.

IV. REACTION MODEL

A. Eikonal theory

The interaction between the projectile (of mass A) and target results in a nucleon being removed from the projectile, leaving a mass $A - 1$ core (or residue). The employed eikonal approximation [24] assumes that, in the small regions where the particles interact, they move in straight-line trajectories

TABLE I. Experimental cross sections for single nucleon knockout from ^{36}Ca to the ground state of the given residue. For each residue, the separation energy S_p and the shell-model single-particle orbital of the particle is given. Also shown are the single-particle cross sections used to extract the spectroscopic factors from the experimental cross sections. The sp cross sections were calculated using the eikonal/HF method [21] and the eikonal/SA method [22]. For the neutron, a calculation was also done using the transfer-to-continuum (TC) method [23]. The last two columns contain the shell-model spectroscopic factors (average of results from USD, USDA, and USDB interactions, which give similar values) and the deduced reduction factor (R_s). The listed uncertainties only include experimental contributions.

Residue	sp orbital	Residue S_p	$\sigma_{\rm exp}$ [mb]	$\sigma_{\rm sp}$[mb]	$S_{\rm deduced}$	$(2j+1)\,S_{\rm deduced}$	$(2j+1)S_{\rm SM}$[a]	R_s
^{35}K	$d_{3/2}$	85 keV	51.1 ± 2.6				3.62	
			Eik/HF	16.2	0.79 ± 0.04	3.19		0.82 ± 0.04
			Eik/SA	11.7	1.09 ± 0.06	4.37		1.14 ± 0.06
^{35}Ca	$s_{1/2}$	1281 keV	5.03 ± 0.46				1.80	
			Eik/HF	11.1	0.23 ± 0.02	0.45		0.24 ± 0.02
			Eik/SA	10.2	0.24 ± 0.02	0.49		0.26 ± 0.02
			TC	10.3	0.25 ± 0.02	0.49		0.26 ± 0.02

[a]The quantities $(2j+1)\,S_{\rm SM}$ in this table is the same as the quantity called C^2S in previous nucleon-knockout papers such as Ref. [4].

of a given impact parameter b at constant velocity. This approximation is valid when the beam energy is high, the scattering angle is small, and the reaction is surface localized [5]. In addition, for composite nuclei, the eikonal approach uses the sudden approximation, which assumes that the removal of the nucleon from the projectile is instantaneous and that the core of the remaining nucleons is undisturbed. The sudden approximation also requires high beam energies so that the interaction time is short compared to the time for any significant motion of the removed nucleon relative to those of the core [25].

To extract a spectroscopic factor from the experimental cross section for a given physical state, it is necessary to calculate single-particle (sp) cross sections ($\sigma_{\rm sp}$) for each contributing sp state. The $\sigma_{\rm sp}$ values shown in Table I are the sum of contributions from stripping (inelastic breakup) and diffractive (elastic) breakup. The ingredients required to calculate $\sigma_{\rm sp}$ in the eikonal model are the core-target and nucleon-target S matrices (S_c and S_n, respectively), and the bound-state wave function for the sp orbital of interest (ϕ).

B. Hartree-Fock constrained calculations

One set of sp cross sections used in this analysis was calculated using the reaction description detailed in Refs. [21] and [5] (referred to as eikonal/HF). Here, the geometries of the optical potentials and the nucleon bound states entering the reaction description [21] are constrained consistently by reference to neutron and proton point densities and the rms radii of the single-particle orbitals obtained using spherical Skyrme SkX Hartree-Fock calculations for the projectile and the reaction residues. Full details of this methodology were given in Ref. [5]. The cross sections calculated using this method were $\sigma_{\rm sp}(-p) = 16.2$ mb for proton knockout and $\sigma_{\rm sp}(-n) = 11.1$ mb for neutron knockout.

Variations on this approach, based on the use of different physical inputs (detailed in Secs. IV B1 and IV B2), were carried out for the neutron knockout using the reaction code MOMDIS [26]. While the reaction theory employed in MOMDIS is the same eikonal model detailed above, this code gave slightly larger values of $\sigma_{\rm sp}$ than those quoted in Table I for the eikonal/HF method. This is due to a different treatment of the nucleon-nucleon (NN) interaction used to generate the elastic S matrices of the nucleon and residues. With either calculation, however, the extracted reduction factors are a small fraction of 1 for the deeply bound valence particles. In addition, by comparing the cross sections calculated with the same reaction code, we can highlight the effect of changing a single input while holding the others fixed. As will be discussed later, all of the input variations resulted in slightly increased sp cross sections (and thus smaller deduced SFs), increasing the discrepancy between the knockout analysis and DOM extrapolations.

1. S matrices

To determine the sensitivity of our results to the details of the S matrix, calculations were repeated for the neutron-knockout reaction using several different methods. These S matrices (shown in Figs. 2 and 3) gave values of $\sigma_{\rm sp}$ that were consistent to within about 20% and are further described below.

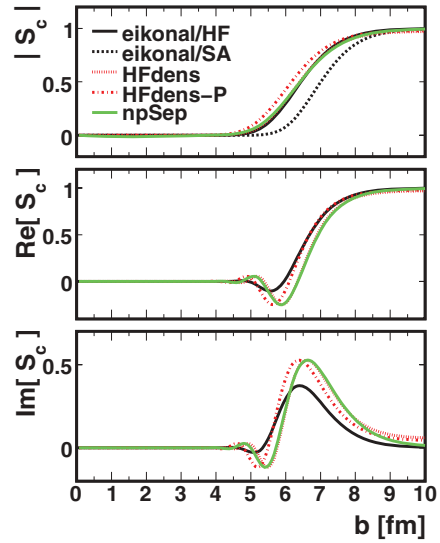

FIG. 2. (Color online) Plot of core-target S matrices (for the neutron-knockout reaction) as a function of impact parameter b, calculated using different method or input. "eikonal/HF" and "eikonal/SA" calculations were done with their respective eikonal reaction codes. The remaining calculations were done with MOMDIS [26]. "HFdens" uses core matter density profiles from Hartree-Fock calculations, "HFdens-P" includes the effect of Pauli blocking, and "npSep" uses separate n and p density profiles. For $S_c \to 1$ (large b) the core survives and for $S_c \to 0$ (small b) the core is destroyed.

The conventional eikonal model approach is to use the $t - \rho\rho$ and $t - \rho$ approximations to the optical potentials for the core-target and nucleon-target S-matrix calculations, respectively. These approximations use the Fourier transform of the target and core (or nucleon) density profiles (ρ_t and ρ_p, respectively) along with an effective nucleon-nucleon (NN) interaction consistent with the free NN cross sections ($\sigma_{\rm NN}$) [26]. Using the MOMDIS code to calculate both the core-target and nucleon-target S matrices in this way, and using the same bound-state wave functions used in the eikonal/HF calculations, single-particle cross sections of $\sigma_{\rm sp}(-p) = 20.8$ mb and $\sigma_{\rm sp}(-n) = 15.6$ mb were obtained for neutron and proton knockout, respectively. (These are larger than the eikonal/HF values, as MOMDIS uses a different treatment of the NN interaction in constructing the S matrix, as described by the authors of Ref. [26].)

The effect of Pauli blocking, which reduces the NN cross sections relative to the free values, results in both S_c and S_n being "pushed in" (i.e., the point at which the S matrix equals 0.5 occurs at a smaller value of b, see Figs. 2 and 3). The net result was to reduce the proton-knockout cross section by about 5%, consistent with the magnitude of the Pauli-blocking effect reported by Bertulani and De Conti [27] for the removal of the $l = 0$ neutron (bound by 1.2 MeV) from ^{15}C. The effect on the neutron-knockout cross section was less than 1%, consistent

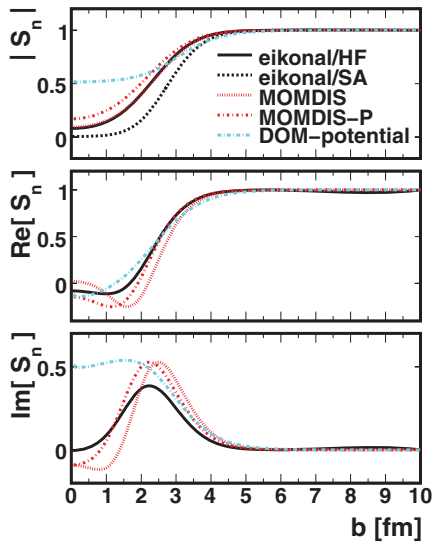

FIG. 3. (Color online) Same as Fig. 2, but for nucleon-target S matrices. "MOMDIS" uses the $t-\rho\rho$ method to calculate the eikonal phase, while "DOM-potential" calculates it directly from an optical potential obtained from the DOM. "MOMDIS-P" includes the effects of Pauli blocking. For $S_n \to 1$ (large b) the nucleon is not removed from the projectile and for $S_n \to 0$ (small b) the nucleon is removed from the projectile.

with results for the deeply bound $l = 0$ neutron removal from ^{34}Ar reported in the same paper.

The S matrix can also be calculated directly from an optical potential. This was done for the nucleon-target S matrices, using potentials obtained from DOM fits to proton and neutron scattering and reaction data for ^{9}Be [28]. (This could not be done for the core-target S matrix as the data required for the fits were not available.) The resulting nucleon-target S matrices differed from those calculated using the $t-\rho$ approximation most strikingly in that they were nonzero as $b \to 0$ (i.e., the DOM includes the finite transparency at small impact parameters that is needed in all optical-model analyses to fit nucleon-scattering data), as can be seen in the S matrix for neutron-knockout plotted in Fig. 3. This difference had a relatively small effect on the calculated cross sections because the nucleon S matrix is multiplied by the core survival amplitude, which goes to zero as $b \to 0$. The proton- and neutron-knockout sp cross sections calculated using the nucleon-target S matrices from the DOM optical potential were $\sigma_{\rm sp}(-p) = 24.49$ mb and $\sigma_{\rm sp}(-n) = 18.56$ mb, respectively—a difference of 15–20% from the MOMDIS results using the double-folding method. To be consistent one should also use wave functions obtained from the DOM, however, the effect of using different wave functions is small, as discussed in the next section.

A more extended density profile results in a smaller knockout cross section due to the decreased core survival probability. This effect is counterbalanced by the corresponding increase in radius of the bound-state orbital. However, one might wonder whether (if the distribution were extended enough) one could obtain calculated cross sections $\sigma_{\rm sp}$, which imply a spectroscopic factor that is consistent with the DOM extrapolation. However, as the tail of the distribution is pushed out radially, the density at the center of the nucleus must decrease to maintain a density distribution that integrates to A. To get a sense of the magnitude of change possible, it is instructive to simply change the density profile (without the counterbalancing change in bound-state radius). Using an extended density distribution that had a central density of 0.125 fm^{-3} (which is 75% of ρ_0, the saturation density) resulted in a calculated cross section $\sigma_{\rm sp}(-n) = 10.7$ mb. An sp cross section of around 4 mb is required in order for the extracted SF to be in line with the DOM extrapolations and transfer results. To obtain a calculated sp cross section this small the density distribution will need to be extended so far that the central density would drop to an unreasonably low value. If one was to change the density profile and bound-state radius in a consistent manner, there is an even smaller effect. Thus one cannot reconcile the differences between the DOM extrapolations and knockout results by any reasonable adjustment of the density distribution used in the knockout calculations.

2. *Wave functions*

The bound-state wave functions were calculated using a Woods-Saxon (WS) potential well or obtained from the DOM. The radius r_0 and diffuseness a of the WS potential are constrained by matching the root-mean-squared radius ($r_{\rm rms}$) of the wave function to HF calculations and the depth V_0 is adjusted to reproduce the physical separation energy of the orbital. There is also a spin-orbit interaction term ($l \cdot s$) with a fixed magnitude of 6 MeV and the same values of r_0 and a as the WS potential [5]. The DOM wave functions are obtained by parameter extrapolation from an analysis of stable calcium isotopes using either a local potential (with a nonlocal correction) or a nonlocal potential [29]. There was very little sensitivity to the use of any of these wave functions [shown in Figs. 4(b) and 5(b), for the ^{36}Ca valence neutron and proton, respectively]. This result is unsurprising since it has been shown [5] that the dependence of $\sigma_{\rm sp}$ on the bound-state wave function is primarily correlated to the $r_{\rm rms}$ of the wave function and these wave functions have similar $r_{\rm rms}$ values. The sp cross sections calculated using these wave functions were within 6% of each other.

The sp cross section is an integral of the S matrices and wave function over the projectile-target spatial coordinate and the nucleon-core spatial coordinate. To gain insight into what parts of the wave functions are sampled in the knockout reaction, we looked at where, in coordinate space, the calculated cross section comes from. In Figs. 4(a) and 5(a) we plot $\frac{d^2\sigma_{\rm str}}{db_n d\rho}$ (calculated using MOMDIS) for the neutron and proton knockout, respectively, as a function of the nucleon impact parameter b_n (the transverse nucleon-target distance, i.e., the component of the nucleon-target distance perpendicular to the beam direction) and the internal projectile coordinate ρ (the transverse nucleon-core distance).

The predicted contributions to the cross-section peak around $b_n = 3$ fm and $\rho = 4$ fm and extend over an oval-shaped spatial region oriented diagonally to the axes, roughly

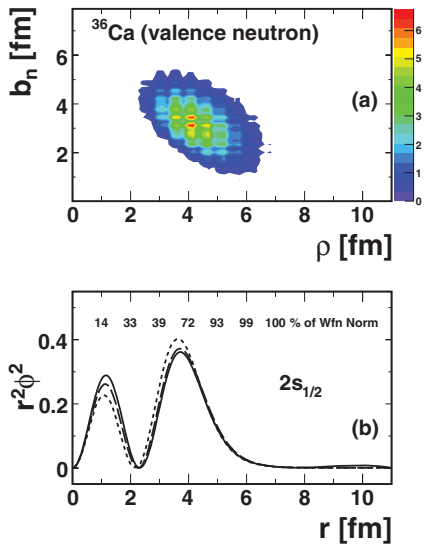

FIG. 4. (Color online) (a) Plot of $\frac{d^2\sigma_{\rm str}}{db_n d\rho}$ for neutron knockout from ^{36}Ca as a function of nucleon impact paramater b_n (nucleon-target transverse distance) and internal projectile radial coordinate ρ (nucleon-core transverse distance). (b) The square of the $s_{1/2}$ bound-state wave function for the valence neutron in ^{36}Ca, multiplied by r^2. The upper scale displays the percentage of the wave-function norm that is within the corresponding radial distance. The three curves are the wave function calculated in a WS potential (solid line), nonlocal potential (long dashed line), and local DOM potential (short dashed line). Calculated using MOMDIS.

where $3 < b_n\,(\text{fm}) < 5.5$ and $2 < \rho\,(\text{fm}) < 6.5$. The shape and orientation of this region reflects the fact that the distance between the projectile and target must be roughly constant—neither too large (or the nucleon is not removed) nor too small (or the core does not survive). So as b_n gets larger (nucleon-target distance increases), ρ must get smaller (nucleon-core distance shrinks) to maintain the projectile center-of-mass distance from the target.

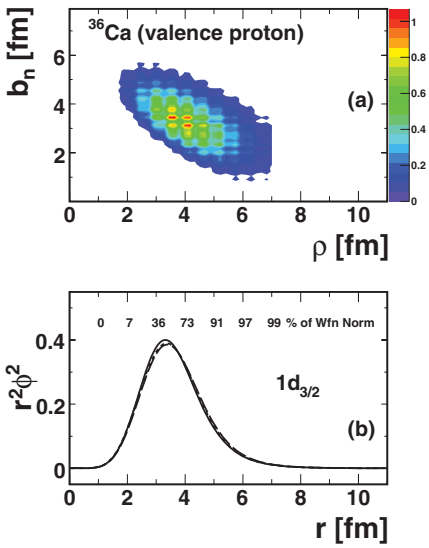

FIG. 5. (Color online) (a) Same as Fig. 4(a), but for knockout from the proton $d_{3/2}$ orbital. (b) Same as Fig. 4(b), but for the $d_{3/2}$ bound-state wave function of the valence proton.

For a given value of ρ, the knockout reaction probes the wave function at radial distances $r \geqslant \rho$. Since the bound-state wave functions for the valence proton and neutron in ^{36}Ca have $r_{\rm rms} \approx 3.8$ fm and $r_{\rm rms} \approx 3.4$ fm, respectively, we conclude that although the knockout reaction is strongest near the surface and does not reach the innermost part of the nucleus it certainly does probe more than just the tail of the wave functions. However, the amount of the wave function probed differs between the neutron and proton removal cases. About 10% of the proton wave function is within $r = 2$ fm and is thus not sampled in the proton-knockout reaction. For the neutron, however, almost 35% of the wave function is within $r = 2$ fm and remains unsampled.

C. Additional calculations

Calculations were also performed using an alternative eikonal approach in which the core-target S matrix is constrained (details below) using the strong absorption radius (these are labeled eikonal/SA) [22]. In addition, for the knockout of the deeply bound neutron, a calculation was done using the transfer-to-continuum (TC) method [23], as implemented in the Appendices of Refs. [30,31]. This method uses asymptotic forms for the wave functions extrapolated inward and so is best applied for reactions that are known to be peripheral.

These methods also employ realistic nucleon-target S matrices [32]. To calculate the n-target S matrix for a ^{9}Be target, a phenomenological optical potential was fitted [22] to the n-target total cross sections. The core-target S matrix was parametrized as a smooth cutoff function of the core-target impact parameter b_c, that is,

$$|S_c|^2 = \exp[-\ln(2)e^{(r_s - b_c)/a_0}], \tag{1}$$

where $a_0 = 0.6$ fm and $r_s = 1.4(A_{\rm proj}^{1/3} + A_{\rm targ}^{1/3})$ fm is the strong absorption radius, according to the traditional strong absorption model [33]. This parametrization leads to reaction cross sections in agreement within 5% to those given by Kox *et al.* [34].

The eikonal/SA method gives single-particle cross sections of $\sigma_{\rm sp}(-p) = 11.7$ mb and $\sigma_{\rm sp}(-n) = 10.3$ mb for proton and neutron knockout, respectively. The TC result for neutron knockout was $\sigma_{\rm sp}(-n) = 10.2$ mb. These neutron sp cross sections are very similar to the results from the eikonal/HF method of Ref. [21], although the proton cross section is 30% smaller.

Some of the difference between the results of the two eikonal methods can perhaps be traced to differences in S_c. The S_c calculated in the eikonal/SA approach is "pushed out" toward higher impact parameters relative to the S_c calculated using the eikonal/HF method (i.e., the point at which $S_c = 0.5$ occurs at a larger value of b_c), as can be seen in Fig. 2. Therefore, the core survival amplitude (and thus the cross section) is smaller. If instead an S matrix similar to that employed in the eikonal/HF approach is used, the calculated

proton-knockout cross section takes the consistent value of $\sigma_{sp}(-p) = 16.0$ mb.

V. ANALYSIS

A. Spectroscopic and reduction factors

In the reactions studied here there is only one bound state in the residue. So assuming the reaction dynamics and the wave function of the removed nucleon are adequately described (for the second of these only the reproduction of r_{rms} is required) then the SF (including the $2j+1$ occupancy factor) can be deduced from the ratio of the inclusive experimental cross section to the sp cross section

$$(2j+1)\,S_{\text{deduced}} \sim \sigma_{\text{exp}}/\sigma_{\text{sp}}. \tag{2}$$

The resulting SFs are given in Table I. As an example, the SF deduced for the valence nucleons in ^{36}Ca using the values from the eikonal/HF approach [21] were $S_{\text{deduced}}(p, d_{3/2}) = 0.79$ and $S_{\text{deduced}}(n, s_{1/2}) = 0.23$. The standard interpretation of these values is that the spectroscopic strength of a single fragment of the correct quantum numbers is only 79% or 23% of the IPM value (for n or p, respectively). (These values are reduced relative to the given SM values by factors of $R_s = 0.82$ and $R_s = 0.24$, respectively.)

In general, the shell-model SF quantifies the contribution of each sp cross section to the theoretical knockout cross section, that is,

$$\sigma_{\text{thy}} = \left(\frac{A}{A-1}\right)^2 \Sigma\,(2j+1)\,S_{\text{SM}}\sigma_{\text{sp}}, \tag{3}$$

where the sum is over all l and j values contributing to the knockout. For the reactions studied here there is only one contribution. The factor $(\frac{A}{A-1})^2$ is a center-of-mass (CM) correction to S_{SM} appropriate for the sd shell [5]. To calculate σ_{thy} one needs to multiply the sp cross section by the theoretical SF. These SF were obtained from shell-model calculations done with the code OXBASH [35], using the "universal" sd-shell (USD) Hamiltonian, as well as the USDA and USDB Hamiltonians [36]. These Hamiltonians gave similar values for these orbitals and the average was used for this analysis. The knocked-out proton was in a $d_{3/2}$ orbital, with $(2j+1)\,S_{\text{SM}} = 3.62$, and the knocked-out neutron was in an $s_{1/2}$ orbital, with $(2j+1)\,S_{\text{SM}} = 1.80$, compared to the extreme sp limits of 4 and 2 for the proton and neutron orbits, respectively.

When there is only one final-state contribution to the cross section (as in the reactions studied here) one can extract an estimate for the SF from R_s

$$S_{\text{deduced}} \sim R_s\,S_{\text{SM}}. \tag{4}$$

The calculated reduction factors $R_s = \frac{\sigma_{\text{exp}}}{\sigma_{\text{thy}}}$ are given in the last column of Table I. The reduction factor for the weakly bound valence proton is consistent with expectations that the SM captures most of the relevant physics, with no more than 20% additional correlations beyond those captured in its model space.

B. Missing spectroscopic strength

A very small spectroscopic factor ($R_s \ll 1$) was deduced for the valence neutron in the ground state of ^{36}Ca. To make sense of this we asked the question: "Where is the rest of the spectroscopic strength?" Since we did not seem to find it in the knockout to the ground state of ^{35}Ca, the next logical place to look would be in the low-lying excited states.

The excited states of ^{35}Ca populated in the experiment are unbound. Neutron decay channels for excited states in these very proton-rich nuclei are negligible, so excited states in ^{35}Ca will proton decay to ^{34}K, which is also unbound and thus will subsequently proton decay to ^{33}Ar before reaching the S800 focal-plane detectors. The proton- and neutron-separation energies of ^{33}Ar are $S_p = 3.3$ MeV and $S_n = 15.3$ MeV, respectively [13]. Thus it is possible that this nuclide is produced in a particle-bound state, which would be observed at the focal plane of the S800.

Therefore, to find the missing spectroscopic strength, it is reasonable to look at the ^{33}Ar residues observed in coincidence with incoming ^{36}Ca. To account for the small spectroscopic factor for the valence neutron in the ground state of ^{36}Ca, one would need to find not only an excess of cross section to this residue (beyond what is expected for other processes, such as direct $-n, -2p$ knockout), but also a cross section that is large compared to that observed for the (bound) ground state of ^{35}Ca. A small cross section would mean either that the spectroscopic strength is far from the Fermi surface or that the extracted spectroscopic factor is incorrect.

The experimental cross section for ^{9}Be(^{36}Ca,^{33}Ar)X was $\sigma(-n, -2p) = 28.6 \pm 1.5$ mb. This is approximately five times larger than the n-knockout cross section. If the spectroscopic factor extracted from the knockout analysis is accurate (i.e., if the 5 mb cross section to ^{35}Ca corresponds to 23% of the spectroscopic strength) then this could, in fact, account for a large portion (if not all) of the missing s-wave strength. For example, even if only half of this cross section is from decay of continuum s states in ^{35}Ca, this would represent an additional 60% of the spectroscopic strength, bringing the total up to 80% of the IPM strength.

VI. DISCUSSION

The measured cross section for knockout of the deeply bound valence neutron in ^{36}Ca is much smaller than the sp cross sections calculated with either the eikonal or the transfer-to-continuum theories. The deduced spectroscopic factor is therefore very small, but consistent with the systematics inferred from previous knockout analyses. A search for the missing spectroscopic strength in the unbound excited states of ^{35}Ca found substantial cross section in the $-n, -2p$ channel, although we cannot determine from our experiment how much of this cross section to ^{33}Ar came from s-wave strength in ^{35}Ca.

If the observed $-n, -2p$ strength is not s wave, then it would lead one to question the extracted SF for the deeply bound neutron. Reasonable adjustments to the eikonal calculation inputs (bound-state wave functions, nuclear density profiles, etc.) did not have a significant effect on the magnitude of the sp cross sections. Thus, if the source of the discrepancy

with DOM extrapolations (and to some extent also the transfer results) is to be found in the knockout analysis, it is likely to lie in our understanding of the reaction mechanism for a system with deeply bound nucleons or with the applicability of an eikonal reaction model to light-target-nucleus-induced knockout reactions at the intermediate energies of the present study. It would prove useful to study these reactions at higher beam energies to explore the robustness of S_{deduced} to changes in beam energy.

However, it could be that a large part of the $-n, -2p$ strength does belong to s-wave neutron removal, followed by proton emission (suggesting strength in the unbound excited states of the $-n$ residue). If this were the case it would give confidence to the extracted SF for the deeply bound neutron and suggest that the SM calculations and DOM extrapolations miss correlations of the valence neutrons due to coupling to protons in the continuum. To further investigate this possibility, one could detect both the emitted proton(s) and the final residue to reconstruct not only the cross section but also the l-wave character of the strength in the near continuum of the neutron-knockout residue.

Knockout cross sections extracted from nucleon-induced knockout [e.g. $(p,2p)$] could also be helpful in ascertaining the source of this discrepancy. Not only would the theory needed to predict knockout cross sections be different than that employed here, but the sampling of the wave function would be intermediate between that of $(e,e'p)$ and that using complex nuclear targets. Needless to say, the spectroscopic strength extracted from $(p,2p)$ reactions would have to agree with those extracted from $(e,e'p)$ for stable nuclei before the value of the nucleon-removal cross sections off stability could be realized.

A very small spectroscopic factor for deeply bound nucleons supports a strong trend in correlations with asymmetry. These enhanced correlations for very asymmetric systems might be understandable on the basis of proximity to the continuum. As the valence level of the weakly bound nucleon approaches the continuum, it can mix strongly with continuum states due to the very small energy difference. The deeply bound valence nucleon can couple to particle-hole excitations of the weakly bound nucleon, shifting spectroscopic strength to lower energies. This could cause an abrupt change in the evolution of the strength of the imaginary potential near the dripline. If this were the case, the present DOM extrapolations would poorly represent dripline behavior. By the same token, standard SM calculations do not include continuum intruder states and would miss correlations due to mixing with such a nearby continuum. In the present case these would be fp-shell proton states.

Recent coupled-cluster work has calculated SFs for a chain of oxygen isotopes with and without the influence of fp-shell continuum states [20]. For the neutron-rich ^{28}O ($N = 20$), they found a drop in the proton SF from $S/S_{\text{IPM}} = 0.7$ to $S/S_{\text{IPM}} = 0.5$ when the continuum was considered. Although these calculations [20] do not fully explain the suppression of SF seen in light-target-nucleus-induced knockout analyses, they may provide a significant step in the needed direction by suggesting that the standard SM calculations are missing low-lying correlations in the continuum. For larger systems, the effect may be enhanced due to the higher density of states. However, mixing with continuum states may be suppressed for cases in which the weakly bound nucleon is a proton (due to the Coulomb barrier) or is not in an s state (due to the centrifugal barrier).

Experimental work by Fallon *et al.* [37] highlights the importance of taking into account fp-shell intruder states. The authors found a much smaller cross section for $2p$ knockout from ^{32}Mg ($N = 20$) than would be expected based on SM calculations with the USD interaction, and show that only a calculation which includes fp-shell occupation could accurately describe the positions of the 2^+ and 4^+ levels in the ^{30}Ne residue. The authors concluded that excitations to fp-shell neutron intruder states contributed significantly to reducing the observed knockout cross section, and the inclusion of mixing with these states led to smaller calculated cross sections (although still larger than experiment). These are the same fp states that come into play for the protons in calcium ($Z = 20$).

VII. CONCLUSION

Cross sections were measured for light-target-nucleus-induced single-nucleon knockout in the proton-rich nucleus ^{36}Ca. Assuming that the radial wave function is reasonable, the small experimental knockout cross section measured for the deeply bound valence neutron (as compared to an eikonal reaction theory) implies a very small spectroscopic factor and supports the strong trend in nucleon correlations with neutron-proton asymmetry that has been observed in similar knockout analyses [4,5]. Such small spectroscopic factors are not predicted by standard SM calculations nor by extrapolations of dispersive optical model fits to nuclear data near stability. Enhanced correlations for very asymmetric systems could be due to strong mixing with continuum states [20]. Continuum intruder levels are not taken into account in standard shell-model calculations and the influence of a close continuum is unlikely to be captured by data sets used to fit the present day DOM potentials.

There is, of course, still the possibility that the simplified eikonal reaction-dynamics description overestimates the sp cross sections for deeply bound nucleons. The reaction model should continue to be tested and it should be shown that the results are reproduced with increasing beam energy. Additional confidence in the reaction theories would be obtained if light-target-nucleus and hydrogen-target knockout data yielded consistent spectroscopic information.

ACKNOWLEDGMENTS

We would like to thank R. Kumar for running eikonal/SA cross-section calculations. This work was supported by the US Department of Energy Grant No. DE-FG02-87ER-40316 (WU), the US National Science Foundation under Contract Nos. PHY-0722822 and PHY-0606007 (NSCL), and the United Kingdom Science and Technology Facilities Council (STFC) under Grant Nos. ST/F012012/1 and ST/J000051/1 (Surrey). This article was abstracted from a doctoral dissertation [38] which contains more details on the analysis.

[1] R. J. Furnstahl and A. Schwenk, J. Phys. G **37**, 064005 (2010).
[2] A. M. Mukhamedzhanov and A. S. Kadyrov, Phys. Rev. C **82**, 051601 (2010).
[3] W. H. Dickhoff and D. Van Neck, *Many-Body Theory Exposed!* (World Scientific, New Jersey, 2005).
[4] A. Gade, D. Bazin, B. A. Brown, C. M. Campbell, J. A. Church, D. C. Dinca, J. Enders, T. Glasmacher, P. G. Hansen, Z. Hu *et al.*, Phys. Rev. Lett. **93**, 042501 (2004).
[5] A. Gade, P. Adrich, D. Bazin, M. D. Bowen, B. A. Brown, C. M. Campbell, J. M. Cook, T. Glasmacher, P. G. Hansen, K. Hosier *et al.*, Phys. Rev. C **77**, 044306 (2008).
[6] B. A. Brown, P. G. Hansen, B. M. Sherrill, and J. A. Tostevin, Phys. Rev. C **65**, 061601 (2002).
[7] R. J. Charity, L. G. Sobotka, and W. H. Dickhoff, Phys. Rev. Lett. **97**, 162503 (2006).
[8] R. J. Charity, J. M. Mueller, L. G. Sobotka, and W. H. Dickhoff, Phys. Rev. C **76**, 044314 (2007).
[9] J. M. Mueller, R. J. Charity, R. Shane, L. G. Sobotka, S. J. Waldecker, W. H. Dickhoff, A. S. Crowell, J. H. Esterline, B. Fallin, C. R. Howell *et al.*, Phys. Rev. C **83**, 064605 (2011).
[10] J. Lee, M. B. Tsang, and W. G. Lynch, Phys. Rev. C **75**, 064320 (2007).
[11] J. Lee, M. B. Tsang, D. Bazin, D. Coupland, V. Henzl, D. Henzlova, M. Kilburn, W. G. Lynch, A. M. Rogers, A. Sanetullaev *et al.*, Phys. Rev. Lett. **104**, 112701 (2010).
[12] F. M. Nunes, A. Deltuva, and J. Hong, Phys. Rev. C **83**, 034610 (2011).
[13] G. Audi and W. Meng (private communication).
[14] D. J. Morrissey, B. M. Sherrill, M. Steiner, A. Stolz, and I. Wiedenhoever, Nucl. Instr. Meth. B **204**, 90 (2003).
[15] D. Bazin, J. A. Caggiano, B. M. Sherrill, J. Yurkon, and A. Zeller, Nucl. Instr. Meth. B **204**, 629 (2003).
[16] D. Weisshaar, A. Gade, T. Glasmacher, G. F. Grinyer, D. Bazin, P. Adrich, T. Baugher, J. M. Cook, C. A. Diget, S. McDaniel *et al.*, Nucl. Instr. Meth. A **624**, 615 (2010).
[17] J. Yurkon, D. Bazin, W. Benenson, D. J. Morrissey, B. M. Sherrill, D. Swan, and R. Swanson, Nucl. Instr. Meth. A **422**, 291 (1999).
[18] V. Pandharipande, I. Sick, and P. deWitt Huberts, Rev. Mod. Phys. **69**, 981 (1997).
[19] M. H. Macfarlane and J. B. French, Rev. Mod. Phys. **32**, 567 (1960).
[20] O. Jensen, G. Hagen, M. Hjorth-Jensen, B. A. Brown, and A. Gade, Phys. Rev. Lett. **107**, 032501 (2011).
[21] J. A. Tostevin, Nucl. Phys. A **682**, 320 (2001).
[22] A. Bonaccorso and G. F. Bertsch, Phys. Rev. C **63**, 044604 (2001).
[23] A. Bonaccorso and D. M. Brink, Phys. Rev. C **38**, 1776 (1988).
[24] P. G. Hansen and J. A. Tostevin, Ann. Rev. Nucl. Part. Sci. **53**, 219 (2003).
[25] F. Carstoiu, E. Sauvan, N. A. Orr, and A. Bonaccorso, Phys. Rev. C **70**, 054602 (2004).
[26] C. A. Bertulani and A. Gade, Comp. Phys. Comm. **175**, 372 (2006).
[27] C. A. Bertulani and C. De Conti, Phys. Rev. C **81**, 064603 (2010).
[28] R. J. Charity (private communication).
[29] W. H. Dickhoff, D. Van Neck, S. J. Waldecker, R. J. Charity, and L. G. Sobotka, Phys. Rev. C **82**, 054306 (2010).
[30] A. Bonaccorso and D. M. Brink, Phys. Rev. C **43**, 299 (1991).
[31] A. Bonaccorso and D. M. Brink, Phys. Rev. C **44**, 1559 (1991).
[32] A. Bonaccorso and F. Carstoiu, Phys. Rev. C **61**, 034605 (2000).
[33] R. Bass, *Nuclear Reactions With Heavy Ions* (Springer, New York, 1980).
[34] S. Kox, A. Gamp, C. Perrin, J. Arvieux, R. Bertholet, J. Bruandet, M. Buenerd, R. Cherkaoui, A. Cole, Y. El-Masri *et al.*, Phys. Rev. C **35**, 1678 (1987).
[35] B. A. Brown, A. Etchegoyen, N. S. Godwin, W. D. M. Rae, W. A. Richter, W. E. Ormand, E. K. Warburton, J. S. Winfield, L. Zhao, and C. H. Zimmerman, MSU-NSCL Report No. 1289 (2004).
[36] B. A. Brown and W. A. Richter, Phys. Rev. C **74**, 034315 (2006).
[37] P. Fallon, E. Rodriguez-Vieitez, A. O. Macchiavelli, A. Gade, J. A. Tostevin, P. Adrich, D. Bazin, M. Bowen, C. M. Campbell, R. M. Clark *et al.*, Phys. Rev. C **81**, 041302 (2010).
[38] R. Shane, Ph.D. thesis, Washington University, 2011.